Gate Tunable Labyrinth Domain Structures in a van der Waals Itinerant Ferromagnet Cr_7Te_8

Kui Meng(孟奎)[1†], Zeya Li(李泽亚)[1†], Yicheng Shen(申艺成)[1†], Xiangyu Bi(毕翔宇)[1], Junhao Rao(饶俊豪)[1], Yuting Qian(钱玉婷)[1], Zhansheng Gao(高战胜)[2], Peng Chen(陈朋)[1], Caiyu Qiu(邱彩玉)[1], Feng Qin(秦峰)[1*], Jinxiong Wu(吴金雄)[3], Feng Luo(罗锋)[3], Junwei Huang(黄俊伟)[1*], and Hongtao Yuan(袁洪涛)[1*]

[1]*National Laboratory of Solid State Microstructures, Jiangsu Key Laboratory of Artificial Functional Materials, College of Engineering and Applied Sciences, and Collaborative Innovation Center of Advanced Microstructures, Nanjing University, Nanjing 210000, China*

[2]*Center for the Physics of Low-Dimensional Materials, Henan Joint International Research Laboratory of New Energy Materials and Devices, School of Physics and Electronics, Henan University, Kaifeng 475004, China*

[3]*Tianjin Key Lab for Rare Earth Materials and Applications, Center for Rare Earth and Inorganic Functional Materials, Smart Sensor Interdisciplinary Science Center, School of Materials Science and Engineering, Nankai University, Tianjin 300350, China*

(Received 11 June 2024; accepted manuscript online 8 August 2024)

Manipulating magnetic domain structure plays a key role in advanced spintronics devices. Theoretical rationale is that the labyrinthine domain structure, normally appearing in ferromagnetic thin films with strong magnetic anisotropy, shows a great potential to increase data storage density for designing magnetic nonvolatile memory and logic devices. However, an electrical control of labyrinthine domain structure remains elusive. Here, we demonstrate the gate-driven evolution of labyrinthine domain structures in an itinerant ferromagnet Cr_7Te_8. By combining electric transport measurements and micromagnetic finite difference simulations, we find that the hysteresis loop of anomalous Hall effect in Cr_7Te_8 samples shows distinct features corresponding to the generation of labyrinthine domain structures. The labyrinthine domain structures are found to be electrically tunable via Li-electrolyte gating, and such gate-driven evolution in Cr_7Te_8 originates from the reduction of the magnetic anisotropic energy with gating, revealed by our micromagnetic simulations. Our results on the gate control of anomalous Hall effect in an itinerant magnetic material provide an opportunity to understand the formation and evolution of labyrinthine domain structures, paving a new route towards electric-field driven spintronics.

DOI: 10.1088/0256-307X/41/9/097501

Magnetic domain structures and their dynamic motions in van der Waals ferromagnets have shown great potentials in magnetic logic and memory devices.[1–9] Theoretically, the motions of magnetic domains are determined by various intrinsic properties of the ferromagnetic materials, such as magnetic anisotropy and saturation magnetization, and those intrinsic properties give rise to a variety of magnetic domain structures therein. Therefore, manipulating magnetic domains can help to study the fundamental principles of the domain formation and evolution, and the microscopic interactions between magnetic moments. Examples of the manipulation of magnetic domains have been demonstrated by applying an external magnetic field,[10–14] or spin-polarized electrical current,[15–26] yet both of these methods have some shortcomings. For the external magnetic field, it can provide uniform magnetic anisotropy to facilitate domain wall movement, while it comes at the cost of substantial energy consumption for generating the required magnetic field, presenting a limitation for nanoscale magnetic devices.[10,12,27] Similarly, for the spin-polarized current, it induces high-speed propagation of domain wall through spin torque, yet it leads to significant energy dissipation due to the high-density current involved.[21] In comparison, an alternative modulation method of magnetic domains by utilizing electrolytes possesses advantages of strong gating effects on the magnetism at low operation voltages. Such an electrolyte-gating method provides a great opportunity to investigate the gate-controlled magnetism and the magnetic domain evolution therein.[28–30] However, research of the evolution of labyrinthine domain structure under gate control remains unexplored.

In this work, we realize the tuning of the hysteresis loop shape of the anomalous Hall effect (AHE) in Cr_7Te_8 nanoflakes through electrolyte gate. We find that the distinct shape of hysteresis loop results from a discernible transformation of the microscopic magnetic domain structures. The sudden jumps of anomalous Hall resistance,

†These authors contributed equally to this work.
*Corresponding authors. Email: htyuan@nju.edu.cn; junweihuang@nju.edu.cn; qinfeng@nju.edu.cn
© 2024 Chinese Physical Society and IOP Publishing Ltd

changing from its saturation value to an intermediate level before the sweeping magnetic field across zero, provide clear evidence of the formation of the labyrinthine domain structure. With an increase in gate voltage, we find that such a labyrinthine domain structure can be electrically induced at low temperatures. By performing micromagnetic simulations, we build corresponding connections between the hysteresis loops and magnetic domain structures. These simulations provide compelling evidence that a reduction in magnetic crystalline anisotropic energy can induce a transformation from single domain to labyrinthine domains in Cr_7Te_8. Our work provides a comprehensive understanding of the pivotal factors governing magnetic domain structures, and facilitates the development of magnetic devices with gate-controlled magnetic domains.

In our experiment, high-quality Cr_7Te_8 nanosheets were grown on mica substrates using a low-pressure chemical vapor deposition (LPCVD) system. Tellurium powder (Te, Alfa Aesar, 99.999%, 0.2 g) and chromium chloride ($CrCl_3$, Alfa Aesar, 99.99%, 20 mg) were utilized as the source materials for chromium and tellurium, respectively. A freshly cleaved fluorophlogopite mica substrate was placed at approximately 1–2 cm behind the $CrCl_3$ powder. The optimal growth conditions included heating the Te and $CrCl_3$ powders to 420 ℃ and 780 ℃, respectively, over a period of 25 min, followed by a 20-min holding time. The reaction was maintained at pressure of 600 Torr, with a carrier argon gas flow of 45 sccm and a hydrogen gas flow of 5 sccm. After the reaction, the system was cooled naturally to room temperature. The as-grown Cr_7Te_8 nanosheets were patterned into a six-terminal Hall-bar device with a side gold pad serving as the electrode for ionic liquid gating. The contact electrodes were written using a maskless laser direct writing system. The contact metal layers (Pd/Au, 5 nm/40 nm) were deposited through thermal evaporation. Low-temperature electronic transport measurements were carried out using an Oxford Instruments TeslatronPT system, equipped with a 12 T superconducting magnet. For the pristine Cr_7Te_8, the magnetoresistance and Hall effect resistance measurements were conducted by zero-field cooling the devices from 300.0 K to 1.5 K at a cooling rate of 1 K/min. The gating experiments were carried out using a solution of $LiClO_4$ and PEO. A mixture of 0.10 g $LiClO_4$ and 0.33 g PEO was dissolved in 5 ml anhydrous methanol. The lithium ions (Li^+) could be driven into the van der Waals gap, facilitating extreme electron doping. The electrolyte was stirred for more than 24 h and heated to 50 ℃ before application. After applying the electrolyte to the Cr_7Te_8 sample surface, the devices were warmed to 370 K for *in situ* annealing for 30 min to remove the organic solvent from the electrolyte.

We chose itinerant ferromagnet Cr_7Te_8 as the target material to realize the gate control of magnetic labyrinthine domain structures for the following three reasons. First, the Cr_7Te_8 is known as a van der Waals itinerant ferromagnet with high Curie temperature and out-of-plane magnetization,[29,31–35] providing a proper material platform to study the magnetic properties based on low-temperature electric transport measurements. Second, the layered van der Waals nature of Cr_7Te_8 facilitates the effective intercalation of metal ions under external gate voltage, which has been confirmed being able to dramatically tune the ferromagnetic properties of Cr_7Te_8.[29] Third, the Cr_7Te_8 is known to exhibit exotic magnetic properties such as the magnetic skyrmionic bubble and labyrinth domain structures with narrow magnetic domain walls,[36] presenting an opportunity of the formation of labyrinthine domain structure therein. These features make Cr_7Te_8 an ideal material to study the gate controllability of magnetic domains, as an exceptionally appealing candidate for the construction of spintronic devices.

To understand the basic magnetic properties of Cr_7Te_8, we measured the longitudinal resistance R_{xx} and the AHE resistance $R_{\rm AHE}$ of Cr_7Te_8 devices with non-encapsulated standard Hall-bar configurations. As shown in Fig. 1(a), the van der Waals itinerant ferromagnet Cr_7Te_8 possesses a layered hexagonal NiAs-type crystal lattice, which can be regarded as the intercalation of Cr (denoted as Cr_i) into the parent compound $CrTe_2$. Figure 1(b) shows the temperature-dependent longitudinal resistance (R_{xx}–T) of two Cr_7Te_8 flakes with different thicknesses (5 nm and 30 nm). For the thicker flake (30 nm), the kink in the R_{xx}–T curve and its first derivative curve at the Curie temperature of 275 K indicates a typical paramagnetic-to-ferromagnetic phase transition. The Curie temperature for the thinner flake (5 nm) is 175 K. Figures 1(c) and 1(d) show the remarkable different experimental AHE hysteresis loops of these two Cr_7Te_8 devices with different thicknesses at 60 K. Specifically, for the thinner Cr_7Te_8 flake (5 nm), the $R_{\rm AHE}$–$\mu_0 H$ curve exhibits rectangular hysteresis loops, suggesting a single-domain configuration characterized by highly anisotropic out-of-plane ferromagnetic ordering. In contrast, for the thicker Cr_7Te_8 flake (30 nm), a discernibly distinct characteristic behavior can be observed in the hysteresis loops. Upon sweeping the magnetic field from negative to positive, the $R_{\rm AHE}$ value suddenly jumps from its saturation value to an intermediate level at a certain magnetic field (denoted as $H_{\rm in}$, as the red circle in Fig. 1(d)). Subsequently, the $R_{\rm AHE}$ changes monotonously and ultimately reaches saturation at a positive high magnetic field. This AHE resistance behavior with a jump can be possibly explained by the transformation of the magnetic domain structure within Cr_7Te_8.[36]

To confirm the validity of the domain simulation results and further build the relationship between the shapes of the hysteresis loop and the magnetic domain structures, we further simulated the hysteresis loop under external magnetic fields ranging from −0.5 T to 0.5 T. As shown in Fig. 1(f), the simulated hysteresis loop for 32-nm-thick Cr_7Te_8 exhibits a sudden jump from the saturation value to an intermediate level. In clear contrast, the simulated hysteresis loop in 2-nm-thick Cr_7Te_8 shows typical rectangular hysteresis loops. The simulated hysteresis loops of both thick and thin Cr_7Te_8 flakes are well-consistent with the experimental results, verifying the reliability of

the micromagnetic simulation results. This underscores that alterations in the hysteresis loop can be ascribed to corresponding changes in the magnetic domain structure within the Cr_7Te_8. Furthermore, the micromagnetic simulation elucidates that the distinctive hysteresis loop observed in the 32-nm-thick Cr_7Te_8 can be attributed to the emergence of labyrinthine domains, providing valuable insights into the underlying physics of this phenomenon.

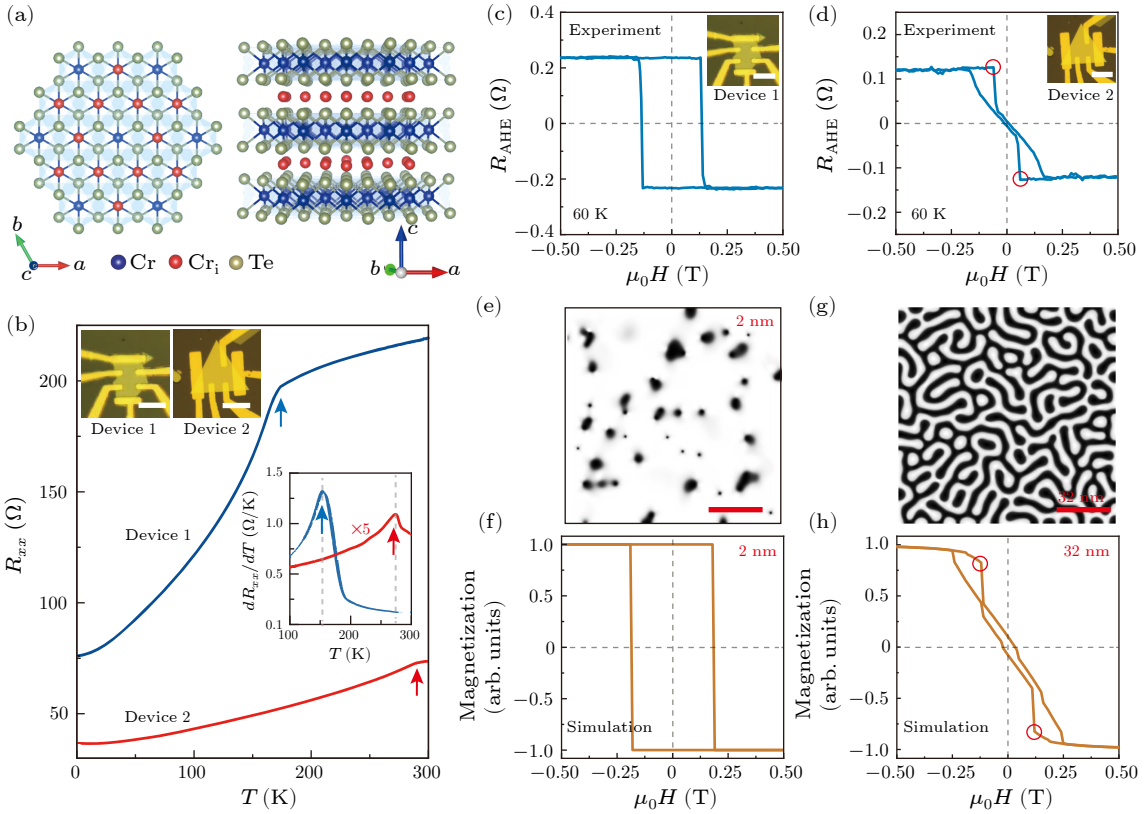

Fig. 1. Crystal structure and thickness-dependent anomalous Hall effect of Cr_7Te_8. (a) Crystal structure of Cr_7Te_8 in the top and side views. The blue and red balls represent Cr atoms constituting the Cr_7Te_8 layers and the intercalated Cr_i atoms, respectively. (b) Temperature-dependent R_{xx} of two Cr_7Te_8 devices with different thicknesses. The upper-left insets show the optical images of two Cr_7Te_8 Hall-bar devices. The thicknesses of the Cr_7Te_8 flakes for devices 1 and 2 are 5 nm and 30 nm, respectively. The scale bar is 5 μm. The right inset shows the first derivative of R_{xx} as a function of temperature. [(c), (d)] Experimental anomalous Hall hysteresis loops of at 60 K for the samples with thicknesses of 5 nm and 30 nm. [(e), (f)] Simulated magnetic domain pattern and the corresponding hysteresis loop of a 32-nm-thick Cr_7Te_8 sample. [(g), (h)] Simulated magnetic domain pattern and the corresponding hysteresis loop of a 2-nm-thick Cr_7Te_8 sample. The scale bars in (e) and (g) are 250 nm. The red circles in (d) and (h) denote the critical magnetic field (H_{in}), where R_{AHE} suddenly jumps from the saturation value to an intermediate level. The parameters used for the simulations in (e)–(g) contain the magnetic exchange constant ($A_{ex} = 1 \times 10^{-12}$ J·m^{-1}), the Landau–Lifshitz damping constant ($\alpha = 0.1$), the saturation magnetization ($M_s = 400 \times 10^3$ A·m^{-1}), and the anisotropy constant ($K = 1 \times 10^5$ J·m^{-3}).

To understand the corresponding magnetic domain structures in Cr_7Te_8 with different thickness and different AHE hysteresis loops, we performed micromagnetic finite difference simulations by using the MuMax3 software package, which has been widely used for characterizing the hysteresis loops and domain structures of magnetic materials.[37] We model the magnetization of Cr_7Te_8 systems with the out-of-plane easy axis by applying the external magnetic field along the z axis. We consider only the z component of the magnetization, and the used parameters contain the thickness, the magnetic exchange constant (A_{ex}), the Landau–Lifshitz damping constant (α), the saturation magnetization (M_s), the anisotropy constant (K) and the external z-oriented magnetic field. Figures 1(e) and 1(g) presents the simulated magnetic domain patterns for 32-nm-thick and 2-nm-thick ferromagnetic Cr_7Te_8, in which the contrasting white and black regions signify two opposite out-of-plane components of magnetization. It is evident that the Cr_7Te_8 flake with 32-nm-thick configuration exhibits an extended labyrinthine domain structure. In contrast, the 2-nm-thick Cr_7Te_8 displays large bubbles domain patterns. Hence, the simulation results demonstrate that the thickness of the magnetic layer exerts a significant influence on its magnetic domain structure. Specifically, a larger thickness gives rise to an intricate magnetic domain configuration, rendering the formation of labyrinthine domains more facile.

Figure 2(a) shows the magnetic-field-dependent AHE

resistance $R_{\rm AHE}$ at various temperatures for the 30-nm-thick Cr_7Te_8 flake. Notably, in contrast to thinner Cr_7Te_8 flake (5 nm) exhibiting a rectangular hysteresis loop below the T_C of 175 K (Fig. S1 in the Supporting Information), the hysteresis loop for thicker Cr_7Te_8 flake only maintains a rectangular shape below 40 K. In an intermediate temperature range of 40 K–150 K, the $R_{\rm AHE}$ hysteresis loops manifest an abrupt transition, characterized by a sudden jump from the saturation value to an intermediate level as the magnetic field is swept upwards. Figure 2(b) shows the evolution of $H_{\rm in}$ with increasing temperature. One can see that the $H_{\rm in}$ value increases progressively until it merges with the saturation field at T_C. Combining with the micromagnetic simulation results in Figs. 1(e)–1(h), this behavior in AHE resistance, featuring a distinctive jump, might be associated with the temperature-dependent magnetic domain structure within Cr_7Te_8.

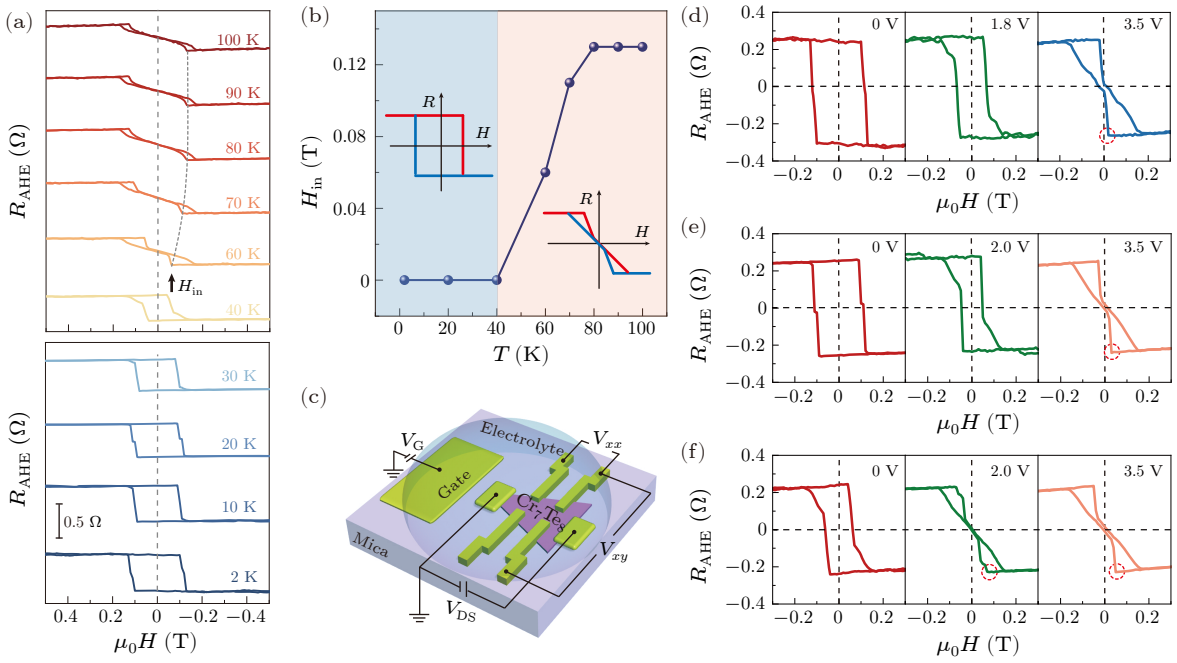

Fig. 2. Gate control of AHE resistance hysteresis loop. (a) AHE resistance $R_{\rm AHE}$ as a function of the out-of-plane magnetic field $\mu_0 H$ at different temperatures for the thicker Cr_7Te_8 sample. The black arrow indicates the sudden jump at $H_{\rm in}$ (60 K). (b) Temperature-dependent $H_{\rm in}$, which indicates that Cr_7Te_8 has different magnetic domain structures in different temperature ranges. The blue (red) curves in the insets represent the data taken by sweeping magnetic field from positive (negative) to negative (positive). (c) Schematic figure of the Hall-bar geometry of the layered ferromagnetic Cr_7Te_8 device with gate-induced Li^+ intercalation. A solution of mixed $LiClO_4$ and PEO was used as the gating electrolyte. (d)–(f) Evolution of AHE resistance hysteresis loop as gate voltage applied at 2 K (d), 20 K (e), and 40 K (f). The red circles represent the occurrence of the sudden jump at $H_{\rm in}$.

To further investigate the influence of band filling in Cr_7Te_8 on the shape of AHE hysteresis loop and corresponding magnetic domain structures, we performed electrolyte-gating experiments to electrically control the AHE by tuning the Fermi level. Figure 2(c) shows a schematic of the electrolyte-gating geometry. A solution of $LiClO_4$ and polyethylene oxide (PEO) was used as the gating electrolyte. At 330 K, lithium ions (Li^+) are electrically driven into the van der Waals gaps of Cr_7Te_8 crystals and finally cause extreme electron doping for tuning the magnetic properties of Cr_7Te_8 flakes. Figure 2(d) illustrates the evolution of the AHE hysteresis loop of a 30-nm-thick Cr_7Te_8 device under different gate voltages at 2 K (more details about the gate tuning of the AHE can be seen from Figs. S2 and S3 in the Supporting Information). In its initial state at a gate voltage of 0 V, the AHE loop has a near-rectangular shape, signifying a stable magnetic state without any abrupt changes or jumps at specific magnetic fields. This implies that the magnetic domain pattern in this 30-nm-thick Cr_7Te_8 sample is a single domain, as presented in the micromagnetic simulation in Figs. 1(e) and 1(f). Upon applying a gate voltage of 1.8 V, the AHE hysteresis loop exhibits discernible jumps at the magnetic fields of $H_{\rm in}$ (± 0.1 T). Specifically, a jump occurs at 0.1 T when sweeping the magnetic field from +1 T to −1 T (in the negative direction), and at −0.1 T when sweeping from −1 T to +1 T (in the positive direction). Notably, the AHE hysteresis loop does not pass through zero magnetic field, indicating that the final labyrinthine domain structure has not yet formed. When a higher gate voltage of 3.5 V is applied, the behavior of the AHE hysteresis loop continues to change. When the magnetic field is scanned in the negative (positive) direction, $H_{\rm in}$ changes from positive (negative) to negative (positive). The AHE hysteresis loop then changes roughly linearly, passes through zero at zero field and finally saturates at a high positive field,

indicating that the final labyrinthine domain structure is formed at this specific gate voltage. The same behavior can also be observed at higher temperatures of 20 K and 40 K [Figs. 2(e) and 2(f)], which confirms that the application of an external gate can indeed alter the magnetic domain structure in magnetic materials, offering a new approach for constructing electronically controlled functional magnetic devices.

To investigate the evolution of the labyrinthine magnetic domains in thicker Cr_7Te_8 under different external magnetic fields, we simulated the magnetic-field-dependent domain structures of Cr_7Te_8 sample [Fig. 3(a)]. In these domain images, the red region denotes the connected domain, commonly known as the labyrinth domain. When the magnetic field is at 0.001 T, the labyrinth domain dominates most of the domain image, suggesting that the overlapping part of the hysteresis loop corresponds to the emergence of the labyrinth domain within the Cr_7Te_8 sample. In addition, if a jump exists, it can lead directly to the fully inverted magnetization state, or to a partial inversion, which requires a further change of the external field to completely revert the magnetization. As the external magnetic field increases (for instance, when $\mu_0 H = 0.04$ T or 0.08 T), the red area starts to shrink, which indicates that the labyrinth domain gradually disappears due to the influence of the magnetic field. When the field strength reaches 0.14 T, the red area essentially vanishes, suggesting that the labyrinth domain has fully transitioned into a state of uniform magnetization (single domain state), as shown in Figs. 3(b)–3(e). Similarly, this phenomenon can also be observed under negative magnetic fields, as shown in Figs. 3(f)–3(h). These results confirm that this unique hysteresis loop exhibits a labyrinth domain structure near a zero magnetic field and gradually transforms into a single domain as the external magnetic field is increased.

To gain deeper insights into the gate-driven hysteresis loop changing and the resulting domain structure transitions, we simulated the magnetic domain structure of Cr_7Te_8 by individually varying the saturated magnetization M_s and the perpendicular magnetic anisotropy energy K since these two crucial magnetic parameters are usually tuned under electrolyte gating. Note that there are many factors that can influence the magnetic domain structure, such as Dzyaloshinskii-Moriya (DM) interaction,[38] magnetic anisotropy, demagnetizing energy, and exchange interaction. Yet, among those various factors, we hypothesize that the magnetic domain changes could be attributed to some of factors, and especially, with M_s and K discussed as potential contributors. Figure 3(i) shows the simulated domain pattern evolution with increasing the saturated magnetization for Cr_7Te_8 with different thicknesses. One can see that only for thicker Cr_7Te_8 samples, the normal magnetic domain structure can gradually transform to the labyrinth domain structure with increasing the saturated magnetization from 300×10^3 A $\cdot$m^{-1} to 600×10^3 A$\cdot$m^{-1}, indicating that the labyrinth domain in Cr_7Te_8 favors to emerge in thicker samples with larger saturated magnetization. Considering that the saturated AHE resistance in Cr_7Te_8 changes slightly with increasing gate voltages in the experiments [Figs. 2(d)–2(f)], we speculate that the gate-induced magnetic domain transition should not be related to the change of saturated magnetization.

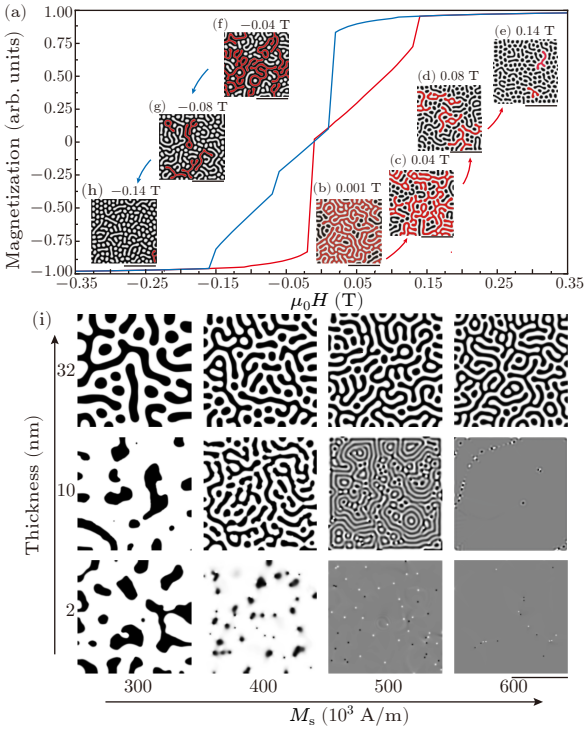

Fig. 3. Micromagnetic simulation of magnetic domain structures of Cr_7Te_8. (a) Simulated hysteresis loop of a Cr_7Te_8 flake and the corresponding domain images (b)–(h) at various applied fields. The red (blue) curve indicates the direction for increasing (decreasing) magnetic fields. (i) Simulated domain pattern as a function of saturation magnetization and thickness for Cr_7Te_8. The scale bar is 500 nm. The parameters used for the simulations contain the magnetic exchange constant ($A_{ex} = 1 \times 10^{-12}$ J$\cdot$m^{-1}), the Landau–Lifshitz damping constant ($\alpha = 0.1$), and the anisotropy constant ($K = 1 \times 10^5$ J $\cdot$m^{-3}). The saturation magnetization in (a)–(h) is $M_s = 800 \times 10^3$ A $\cdot$m^{-1}. The saturation magnetization in (i) corresponds to the X-axis values in units of 10^3 A $\cdot$m^{-1}.

Figure 4 performs a series of simulations including the hysteresis loop and magnetic domain structure of the Cr_7Te_8 system under various magnetic anisotropy conditions. The magnetic anisotropy energy decreases obviously with an increase in gate voltage, as demonstrated in another famous van der Waals itinerant ferromagnet Fe_5GeTe_2.[28] The evolution of the Cr_7Te_8 system is driven by a reduction in magnetic anisotropy, which is a pivotal parameter in its magnetic domain structure. When magnetic anisotropy is high ($K = 4 \times 10^5$ J$\cdot$m^{-3} or 2×10^5 J $\cdot$m^{-3}), the simulation results demonstrate a substantial, nearly rectangular hysteresis loop and no finite magnetization jump (H_{in}) are observed, as depicted in Figs. 4(a) and 4(c). Correspondingly, the simulated magnetic domains exhibit stripy and circular domain patterns, as shown in Figs. 4(b) and 4(d). However, as the magnetic anisotropy decreases to 0.8×10^5 J$\cdot$m^{-3}, the sudden jump of R_{AHE}

at H_{in} starts to emerge in the hysteresis loop, as illustrated in Fig. 4(e). As a result, the magnetic domains transform from their original stripe-like and bubble-like domains to a newly formed labyrinthine domain [Fig. 4(f)]. Upon further reduction of the magnetic anisotropy to $0.5 \times 10^5\,\mathrm{J{\cdot}m^{-3}}$, the simulated hysteresis loop matches well with the experimental shape for 30-nm-thick Cr_7Te_8 in Fig. 1, and a pronounced jump in magnetization intensity is observed during the magnetic field sweep [Fig. 4(g)]. Likewise, the corresponding magnetic domain simulation vividly displays a distinct labyrinthine domain structure [Fig. 4(h)]. These results provide compelling evidence that the magnetic anisotropy change might be responsible for the gate-induced hysteresis loop change and the resulting magnetic domain transitions in Cr_7Te_8. In the itinerant magnetic CrTe system, super-exchange interaction between Cr atoms is expected to be dominant in determining the overall magnetism.[39] Theoretically, the magnetic anisotropy is influenced by the local environment surrounding the magnetic sites, including local symmetries within the atomic monolayer, specific electronic states at the Fermi level, and exchange interactions between neighboring magnetic sites.[40] Notably, the interaction between itinerant electrons and local magnetic moments can effectively screen these local moments and tune the ferromagnetic behavior. The degree of this shielding is determined by the density of states of electrons at the Fermi level and is amenable to modulation through gating. Generally, gating can change the position of the Fermi level, altering the ratio of itinerant to localized electrons, which typically leads to changes in the exchange mechanism. Examples have been demonstrated in van der Waals ferromagnetic Fe_5GeTe_2 that the magnetic anisotropy can also be continuously manipulated by adjusting the density of states near the Fermi level via electrolyte gate.[28] In our Cr_7Te_8 case, such a gate control of magnetic anisotropy leads to a profound influence on the emergence of the unique labyrinthine domains, providing a unique strategy to modulate the magnetic domain structures in the magnetic materials.

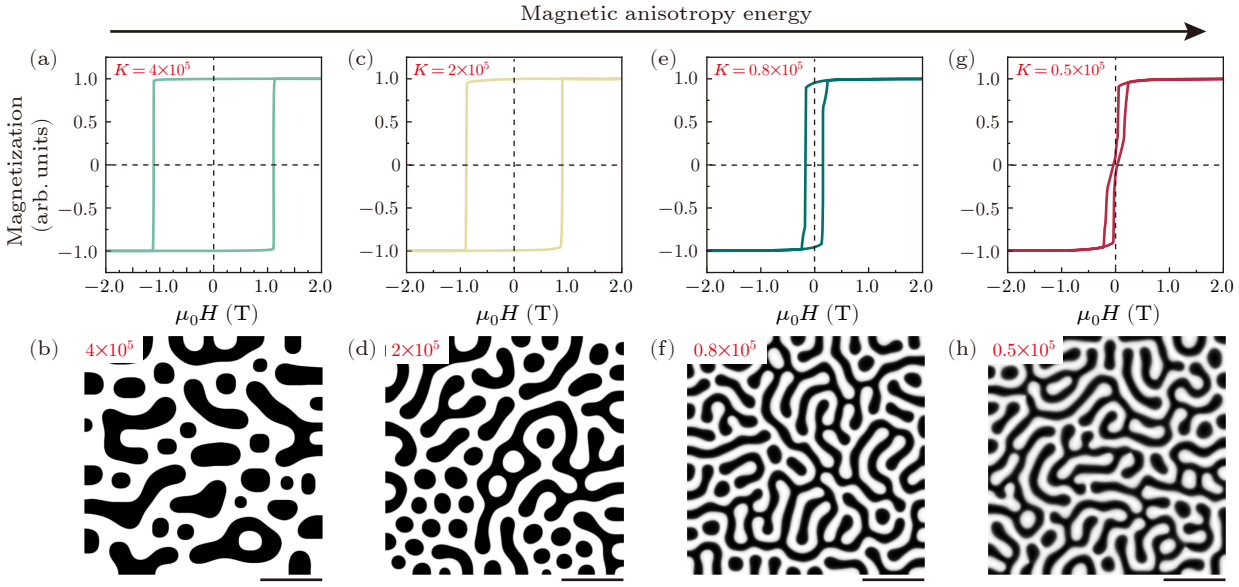

Fig. 4. Micromagnetic simulation for a 32-nm-thick Cr_7Te_8 flake by varying magnetic anisotropy. (a)–(h) Simulated hysteresis loop and domain pattern in the Cr_7Te_8 system with magnetic anisotropy at $4 \times 10^5\,\mathrm{J{\cdot}m^{-3}}$ [(a), (b)], $2 \times 10^5\,\mathrm{J{\cdot}m^{-3}}$ [(c), (d)], $0.8 \times 10^5\,\mathrm{J{\cdot}m^{-3}}$ [(e), (f)], and $0.5 \times 10^5\,\mathrm{J{\cdot}m^{-3}}$ [(g), (h)]. The scale bar is 250 nm. The parameters used for the simulations contain the magnetic exchange constant ($A_{ex} = 1 \times 10^{-12}\,\mathrm{J{\cdot}m^{-1}}$), the Landau–Lifshitz damping constant ($\alpha = 0.1$), and the saturation magnetization ($M_s = 500 \times 10^3\,\mathrm{A{\cdot}m^{-1}}$). The anisotropy constant is listed in the left upper corner of each panel.

In summary, we have demonstrated the gate manipulation of magnetic domain structures in itinerant ferromagnetic Cr_7Te_8. By combining the AHE measurements and the micromagnetic simulations, we have built the connection between the distinctive hysteresis loop of the AHE resistance and the formation of labyrinthine domains in Cr_7Te_8. Our micromagnetic simulations reveals that the magnetic layer thickness and saturated magnetization can significantly influence the shape of the AHE hysteresis loop. More importantly, the gate tuning effect on the density of states near the Fermi level can modulate the magnetic anisotropy energy, thereby driving the transition of magnetic domains from bubble to labyrinth patterns. Our work demonstrates the capability to manipulate magnetic domains via external gate, paving the way for potential applications in magnetic logic and memory devices.

Acknowledgments. This work was supported by the National Natural Science Foundation of China (Grant Nos. 92365203, 52072168, 51861145201, 52302180, and 12204232), the National Key Research and Development Program of China (Grant No. 2021YFA1202901), the Science and Technology Development Project of Henan

Province (Grant No. 242102230140), and the China Postdoctoral Science Foundation (Grant No. 2024M750775).

References

[1] Allwood D A, Xiong G, Faulkner C C, Atkinson D, Petit D, and Cowburn R P 2005 *Science* **309** 1688

[2] Chappert C, Fert A, and Van Dau F N 2007 *Nat. Mater.* **6** 813

[3] Lavrijsen R, Lee J H, Fernández-Pacheco A, Petit D C M C, Mansell R, and Cowburn R P 2013 *Nature* **493** 647

[4] Parkin S S P, Hayashi M, and Thomas L 2008 *Science* **320** 190

[5] Omari K A and Hayward T J 2014 *Phys. Rev. Appl.* **2** 044001

[6] Diegel M, Glathe S, Mattheis R, Scherzinger M, and Halder E 2009 *IEEE Trans. Magn.* **45** 3792

[7] Borie B, Kehlberger A, Wahrhusen J, Grimm H, and Kläui M 2017 *Phys. Rev. Appl.* **8** 024017

[8] Mattheis R, Diegel M, Hubner U, and Halder E 2006 *IEEE Trans. Magn.* **42** 3297

[9] Cui Q, Liang J, Zhu Y, Yao X, and Yang H 2023 *Chin. Phys. Lett.* **40** 037502

[10] Beach G S D, Nistor C, Knutson C, Tsoi M, and Erskine J L 2005 *Nat. Mater.* **4** 741

[11] Nakatani Y, Thiaville A, and Miltat J 2003 *Nat. Mater.* **2** 521

[12] Atkinson D, Allwood D A, Xiong G, Cooke M D, Faulkner C C, and Cowburn R P 2003 *Nat. Mater.* **2** 85

[13] Wang R, Shang Y X, Wu R, Yang J B, and Ji Y 2016 *Chin. Phys. Lett.* **33** 047502

[14] Liu J, Wang Z, Xu T, Zhou H, Zhao L, Je S G, Im M Y, Fang L, and Jiang W 2022 *Chin. Phys. Lett.* **39** 017501

[15] Hayashi M, Thomas L, Moriya R, Rettner C, and Parkin S S P 2008 *Science* **320** 209

[16] Chiba D, Yamada G, Koyama T, Ueda K, Tanigawa H, Fukami S, Suzuki T, Ohshima N, Ishiwata N, Nakatani Y, and Ono T 2010 *Appl. Phys. Express* **3** 073004

[17] Yamaguchi A, Ono T, Nasu S, Miyake K, Mibu K, and Shinjo T 2004 *Phys. Rev. Lett.* **92** 077205

[18] Yamanouchi M, Chiba D, Matsukura F, and Ohno H 2004 *Nature* **428** 539

[19] Tatara G and Kohno H 2004 *Phys. Rev. Lett.* **92** 086601

[20] Vernier N, Allwood D A, Atkinson D, Cooke M D, and Cowburn R P 2004 *Europhys. Lett.* **65** 526

[21] Saitoh E, Miyajima H, Yamaoka T, and Tatara G 2004 *Nature* **432** 203

[22] Thiaville A, Nakatani Y, Miltat J, and Suzuki Y 2005 *Europhys. Lett.* **69** 990

[23] Kläui M, Vaz C A F, Bland J A C, Wernsdorfer W, Faini G, Cambril E, Heyderman L J, Nolting F, and Rüdiger U 2005 *Phys. Rev. Lett.* **94** 106601

[24] Thomas L, Hayashi M, Jiang X, Moriya R, Rettner C, and Parkin S S P 2006 *Nature* **443** 197

[25] Miron I M, Moore T, Szambolics H, Buda-Prejbeanu L D, Auffret S, Rodmacq B, Pizzini S, Vogel J, Bonfim M, Schuhl A, and Gaudin G 2011 *Nat. Mater.* **10** 419

[26] Jin Z, Song M, Fang H, Chen L, Chen J, and Tao Z 2022 *Chin. Phys. Lett.* **39** 108502

[27] Rushforth A W, Rowan-Robinson R, and Zemen J 2020 *J. Phys. D* **53** 164001

[28] Tang M, Huang J, Qin F, Zhai K, Ideue T, Li Z, Meng F, Nie A, Wu L, Bi X, Zhang C, Zhou L, Chen P, Qiu C, Tang P, Zhang H, Wan X, Wang L, Liu Z, Tian Y, Iwasa Y, and Yuan H 2023 *Nat. Electron.* **6** 28

[29] Meng K, Li Z, Gao Z, Bi X, Chen P, Qin F, Qiu C, Xu L, Huang J, Wu J, Luo F, and Yuan H 2024 *InfoMat* **6** e12524

[30] Deng Y, Yu Y, Song Y, Zhang J, Wang N Z, Sun Z, Yi Y, Wu Y Z, Wu S, Zhu J, Wang J, Chen X H, and Zhang Y 2018 *Nature* **563** 94

[31] Hashimoto T and Yamaguchi M 1969 *J. Phys. Soc. Jpn.* **27** 1121

[32] Akram M and Nazar F M 1983 *J. Mater. Sci.* **18** 423

[33] Chen B W, Wu X K, Liao Z Y, Fu Z D, Xu B, Wang M, and Shen B 2024 arXiv:2404.00659 [cond-mat.mtrl-sci]

[34] Gao Z, Tang M, Huang J, Chen J, Ai W, Wu L, Dong X, Ma Y, Zhang Z, Zhang L, Du Y, Fu H, Yuan H, Wu J, and Luo F 2022 *Nano Res.* **15** 3763

[35] Miao W T, Zhen W L, Lu Z, Wang H N, Wang J, Niu Q, and Tian M L 2024 *Chin. Phys. Lett.* **41** 067501

[36] Liu J, Ding B, Liang J, Li X, Yao Y, and Wang W 2022 *ACS Nano* **16** 13911

[37] Vansteenkiste A, Leliaert J, Dvornik M, Helsen M, Garcia-Sanchez F, and Van Waeyenberge B 2014 *AIP Adv.* **4** 107133

[38] Zhang H, Raftrey D, Chan Y T, Shao Y T, Chen R, Chen X, Huang X, Reichanadter J T, Dong K, Susarla S, Caretta L, Chen Z, Yao J, Fischer P, Neaton J B, Wu W, Muller D A, Birgeneau R J, and Ramesh R 2022 *Sci. Adv.* **8** eabm7103

[39] Yang J, Zhu C, Deng Y, Tang B, and Liu Z 2023 *iScience* **26** 106567

[40] Bi X, Qiu C, Qin F, Huang J, and Yuan H 2023 *Adv. Phys. Res.* **2** 2200106